

# Object Detection in Videos by High Quality Object Linking

Peng Tang<sup>†\*</sup> Chunyu Wang<sup>‡</sup> Xinggang Wang<sup>†</sup> Wenyu Liu<sup>†</sup> Wenjun Zeng<sup>‡</sup> Jingdong Wang<sup>‡</sup>

<sup>†</sup>School of EIC, Huazhong University of Science and Technology <sup>‡</sup>Microsoft Research Asia

{pengtang, xgwang, liuwu}@hust.edu.cn

{chnuwa, wezeng, jingdw}@microsoft.com

## Abstract

Compared with object detection in static images, object detection in videos is more challenging due to degraded image qualities. An effective way to address this problem is to exploit temporal contexts by linking the same object across video to form tubelets and aggregating classification scores in the tubelets. In this paper, we focus on obtaining high quality object linking results for better classification. Unlike previous methods that link objects by checking boxes between neighboring frames, we propose to link in the same frame. To achieve this goal, we extend prior methods in following aspects: (1) a cuboid proposal network that extracts spatio-temporal candidate cuboids which bound the movement of objects; (2) a short tubelet detection network that detects short tubelets in short video segments; (3) a short tubelet linking algorithm that links temporally-overlapping short tubelets to form long tubelets. Experiments on the ImageNet VID dataset show that our method outperforms both the static image detector and the previous state of the art. In particular, our method improves results by 8.8% over the static image detector for fast moving objects.

## 1. Introduction

Detecting objects in static images [5, 6, 22, 24, 25, 35, 31] has achieved significant progress due to the emergence of deep convolutional neural networks (CNNs) [11, 18, 19, 29]. However, object detection in videos brings additional challenges due to degraded image qualities, *e.g.* motion blur and video defocus, leading to unstable classifications for the same object across video. Therefore, many research efforts have been allocated to video object detection by exploiting temporal contexts [8, 3, 17, 16, 15, 37, 36], especially after the introduction of the ImageNet video object detection (VID) challenge.

Many previous methods exploit temporal contexts by linking the same object across video to form tubelets and aggregating classification scores in the tubelets [8, 17, 16,

3]. They first use static image detectors to detect objects in each frame, and then link these detected objects by checking object boxes between neighboring frames, according to the spatial overlap between object boxes in different frames [8] or predicting object movements between neighboring frames [17, 16, 15, 3]. Very promising results are obtained by these methods.

However, the same object changes its locations and appearances in neighboring frames due to object motion, which may make the spatial overlap between boxes of the same object in neighboring frames not sufficient enough or the predicted object movements not accurate enough. This influences the quality of object linking, especially for fast moving objects. By contrast, in the same frame, it is obvious that two boxes correspond to the same object if they have sufficient spatial overlaps. Inspired by these facts, we propose to link objects in the same frame instead of neighboring frames for high quality object linking.

In our method, a long video is first divided into some temporally-overlapping short video segments. For each short video segment, we extract a set of cuboid proposals, *i.e.* spatio-temporal candidate cuboids which bound the movement of objects, by extending the region proposal network for static images [25] to a cuboid proposal network for short video segments. The objects across frames lying in a cuboid are regarded as the same object.

For each cuboid proposal, we adapt the Fast R-CNN [5] to detect short tubelets. More precisely, we compute the precise box locations and classification scores for each frame separately, forming a short tubelet representing the linked object boxes in the short video segment. We compute the classification score of the tubelet, by aggregating the classification scores of the boxes across frames. In addition, to remove spatially redundant short tubelets, we extend the standard non-maximum suppression (NMS) with a tubelet overlap measurement, which prevents tubelets from breaking that may happen in frame-wise NMS. Considering short range temporal contexts by short tubelets benefits detection, see Fig. 1 (b).

Finally, we link the short tubelets with sufficient overlap across temporally-overlapping short video segments. If two

\*This work was done during Microsoft Research Asia internship.

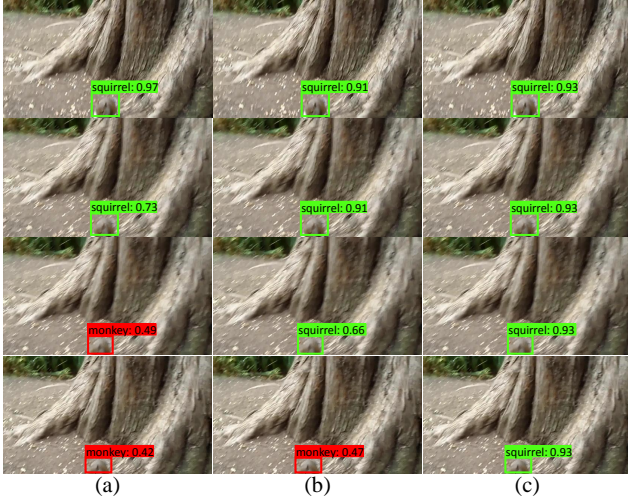


Figure 1. (a) Static image detection: only the detections in the first two frames are correct. (b) Short tubelet detection: the detection in the third frame becomes correct due to object linking between the second and third frame. (c) Short tubelet linking: The detections in all the frames are correct due to short tubelet linking. Here the short video segment length is 2. For each frame, we only show the top-scoring box, where green/red boxes correspond to success/failure examples.

boxes, which are from the temporally-overlapping frame (*i.e.* the same frame) of two neighboring short tubelets, have sufficient spatial overlap, the two corresponding short tubelets are linked together and merged. We exploit the object linking to improve the classification quality by boosting the classification scores for positive detections through aggregating the classification scores of the linked tubelets. As shown in Fig. 1 (c), the detection results can be further improved by considering long range temporal contexts.

Elaborate experiments are conducted on the ImageNet VID dataset [26]. Our method obtains mAP 74.5% training on the VID and 80.6% training on the mixture of VID and DET. The results outperform both the static image detector and the previous best performed methods. In particular, our method obtains 8.8% absolute improvement compared with the static image detector for fast moving objects.

## 2. Related work

The task of object detection in both images [4, 5, 6, 9, 21, 22, 32, 24] and videos [3, 15, 16, 36, 37] has been widely studied in the literature. We mainly review related works on video object detection and classify them into three categories by how they use the temporal contexts.

**Feature Propagation w/o Object Linking.** In [36], the features of the current frame are augmented by aggregating the features propagated from the neighboring frames based on the pixel-wise correspondences which are established by computing the optical flows [2]. Feature propaga-

tion is also exploited in [37] to speed up the object detection. The authors propose to compute the feature maps (using a very deep network with high computation cost) for the key frames and propagate the features to non-key frames by computing the optical flows using a shallow network which takes less time. These methods are different from ours because they do not perform object linking.

**Feature Propagation w/ Object Linking.** The tubelet proposal network [15] computes tubelets by first generating static object proposals in the first frame and then predicting their relative movements in following frames. The features of the boxes in the tubelets are propagated to each box for classification by using a CNN-LSTM network. Unlike their method, we link objects in the same frame and propagate box scores instead of features across frames. Besides, we directly generate the spatio-temporal cuboid proposals for video segments rather than per-frame proposals in [15].

**Score Propagation w/ Object Linking.** The method in [16, 17] proposes two kinds of object linking. The first one tracks the detected box in current frame to its neighboring frames to augment their original detections for higher object recall. The scores are also propagated to improve classification accuracy. The linking is based on the mean optical flow vector within boxes. The second one links objects into long tubelets using the tracking algorithm [33] and then adopts a classifier to aggregate the detection scores in the tubelets. The Seq-NMS method [8] links objects by checking the spatial overlap between boxes in neighboring frames without considering the motion information and then aggregates the scores of the linked objects for the final score. The method in [3] simultaneously predicts the object locations in two frames and also the object movements from the preceding frame to the current frame. Then they use the movements to link the detected objects into tubelets. The object detection scores in the same tubelet is reweighed by aggregating the scores in some manner from the scores in that tubelet.

Our method belongs to the third category. The main contribution of our work is that we link objects in the same frame instead of neighboring frames in previous methods [8, 17, 16, 3, 15]. In addition, to achieve our goal, we develop a series of methods such as cuboid proposal network which have not been explored in previous methods.

## 3. Our approach

The task of video object detection is to infer the locations and classes of the objects in each frame of a video  $\{\mathbf{I}^1, \mathbf{I}^2, \dots, \mathbf{I}^N\}$ . To obtain high quality object linking, our method proposes to link objects in the same frame, which can be used to improve the classification accuracy.

Given a video divided into a series of temporally-overlapping short video segments as the input, our method consists of three stages: (1) Cuboid proposal generation for

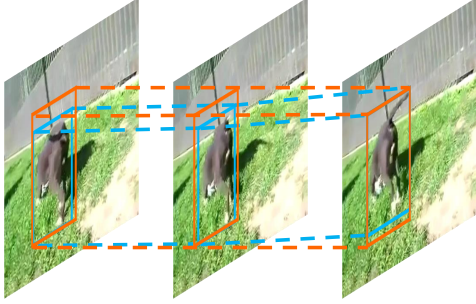


Figure 2. The orange cuboid, bounding the movement of the object, is the target of the cuboid proposal stage. The tubelet, composed of the blue object boxes in the video segment, is the target of the short tubelet objection stage.

a short video segment. This stage aims to generate a set of cuboids (containers) which bound the same object across frames as shown in Fig. 2. See Section 3.1. (2) Short tubelet detection for a short video segment. For each cuboid proposal, the goal is to regress and classify a short tubelet which is a sequence of bounding boxes with each box localizing the object in one frame. The spatially-overlapping short tubelets are removed by tubelet non-maximum suppression. The short tubelet is a representation for linked objects across frames in a short video segment, as illustrated in Fig. 2. See Section 3.2. (3) Short tubelet linking for the whole video. This stage, depicted in Fig. 3, links the temporally-overlapping short tubelets to link objects in the whole video, and refines the classification scores of the linked tubelets. See Section 3.3. The first two stages, cuboid proposal generation and short tubelet detection, generate temporally-overlapping short tubelets, and thus ensure that we can link objects in the temporally-overlapping frame (*i.e.* the same frame) in the short tubelet linking stage.

### 3.1. Cuboid Proposal Generation

The ground truth bounding cuboid of the objects in a short video segment, containing  $K$  frames  $\{\mathbf{I}^t, \mathbf{I}^{t+1}, \dots, \mathbf{I}^{t+K-1}\}$ , is defined as follows. Let  $\tilde{\mathbf{b}}$  be the  $2D$  bounding box of the tubelet  $\tilde{\mathcal{T}} = (\tilde{\mathbf{b}}^t, \tilde{\mathbf{b}}^{t+1}, \dots, \tilde{\mathbf{b}}^{t+K-1})$ , a series of all ground truth boxes in the  $K$  frames,

$$\tilde{\mathbf{b}} = \text{BoundingBox}(\tilde{\mathbf{b}}^t, \tilde{\mathbf{b}}^{t+1}, \dots, \tilde{\mathbf{b}}^{t+K-1}). \quad (1)$$

Here,  $\tilde{\mathbf{b}}^\tau = (x^\tau, y^\tau, w^\tau, h^\tau)$  in frame  $\tau$ , denoting the horizontal and vertical center coordinates and its width and height, is the ground truth box of frame  $\tau$ . The bounding cuboid in our method is just a collection of  $K$   $\tilde{\mathbf{b}}$ s:  $\tilde{\mathbf{c}} = (\tilde{\mathbf{b}}, \tilde{\mathbf{b}}, \dots, \tilde{\mathbf{b}})$ , and thus simplified as a  $2D$  box  $\tilde{\mathbf{b}}$ . Fig. 2 provides the examples of the cuboid and the tubelet in a short video segment.

We modify the region proposal network (RPN) method in Faster R-CNN [25] and introduce the cuboid proposal

network (CPN) method for computing cuboid proposals. Unlike the conventional RPN where the input is usually a single image, our method takes the  $K$  frames as the input to the CPN. The output is a set of  $whk$  cuboid proposals, regressed from a  $w \times h$  spatial grid, where there are  $k$  reference boxes at each location, and each cuboid proposal is associated with an objectness score.

### 3.2. Short Tubelet Detection

We use the  $2D$  form of the cuboid proposal, as the  $2D$  box (region) proposal for each frame in this segment, which is classified and refined for each frame separately.

Considering a frame  $\mathbf{I}^\tau$  in this segment, we follow Fast R-CNN [5] to refine the box and compute the classification score. We start with a RoI pooling operation, where the input is a  $2D$  region proposal  $\mathbf{b}$  and the response map of  $\mathbf{I}^\tau$  obtained through a CNN. The RoI pooling result is fed into a classification layer, outputting a  $\{C+1\}$ -dimensional classification score vector  $\mathbf{y}^\tau$ , where  $C$  is the number of categories and 1 corresponds to the background, as well as a regression layer, from which the refined box is obtained.

The resulting  $K$  refined boxes for the  $K$  frames form the short tubelet detection result over this segment,  $\mathcal{T} = (\mathbf{b}^t, \mathbf{b}^{t+1}, \dots, \mathbf{b}^{t+K-1})$ . The classification score of this tubelet is an aggregation of the scores over all the frames,

$$\bar{\mathbf{y}} = \text{aggregation}(\mathbf{y}^t, \mathbf{y}^{t+1}, \dots, \mathbf{y}^{t+K-1}), \quad (2)$$

where  $\text{aggregation}(\cdot)$  could be a mean operation. We empirically find that  $\text{Aggregation}(\cdot) = \frac{1}{2}(\text{mean}(\cdot) + \text{max}(\cdot))$  performs the best.

To remove spatial redundant short tubelets, we extend the standard non-maximum suppression (NMS) algorithm to a tubelet NMS (T-NMS) algorithm to remove spatially-overlapping short tubelets in the same segment. This strategy prevents tubelets from breaking by frame-wise NMS which removes  $2D$  boxes for each frame independently. The main point lies in how to measure the spatial overlap between two tubelets. We define it on the base of the overlap between the boxes in the same frame. Given two tubelets,  $\mathcal{T}_i = (\mathbf{b}_i^t, \mathbf{b}_i^{t+1}, \dots, \mathbf{b}_i^{t+K-1})$  and  $\mathcal{T}_j = (\mathbf{b}_j^t, \mathbf{b}_j^{t+1}, \dots, \mathbf{b}_j^{t+K-1})$ , the spatial overlap is computed as

$$\text{overlap}(\mathcal{T}_i, \mathcal{T}_j) = \min_{\tau=t, t+1, \dots, t+K-1} \text{IoU}(\mathbf{b}_i^\tau, \mathbf{b}_j^\tau), \quad (3)$$

where  $\text{IoU}(\mathbf{b}_i^\tau, \mathbf{b}_j^\tau)$  is the intersection over union between  $\mathbf{b}_i^\tau$  and  $\mathbf{b}_j^\tau$  for frame  $\tau$ . We choose this measurement because two short tubelets are not the same even if only one pair of corresponding boxes do not have sufficient overlap.

### 3.3. Short Tubelet Linking

Our method divides a video into a series of temporally-overlapping short video segments of length  $K$  with stride

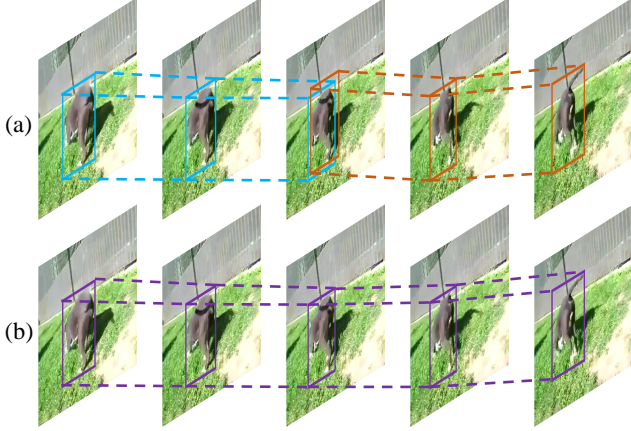


Figure 3. Illustration of short tubelet linking. Boxes with the same color belong to the same tubelet. The short tubelets (a) from two temporally-overlapping video segments are linked together to form new long tubelets (b).

$K - 1$ :

$$\mathcal{S}^1 = (\mathbf{I}^1, \mathbf{I}^2, \dots, \mathbf{I}^K), \quad (4)$$

$$\mathcal{S}^2 = (\mathbf{I}^K, \mathbf{I}^{K+1}, \dots, \mathbf{I}^{2K-1}), \quad (5)$$

$$\dots \dots \quad (6)$$

$$\mathcal{S}^M = (\mathbf{I}^{(M-1)K-M+2}, \dots, \mathbf{I}^{MK-M+1}). \quad (7)$$

Considering two temporally-overlapping short tubelets: the  $i$ th tubelet from the  $m$ th segment and the  $i'$ th tubelet from the  $(m + 1)$ th segment:

$$\mathcal{T}_i^m = (\mathbf{b}_i^{t_m}, \mathbf{b}_i^{t_m+1}, \dots, \mathbf{b}_i^{t_m+K-1}),$$

$$\mathcal{T}_{i'}^{m+1} = (\mathbf{b}_{i'}^{t_m+K-1}, \mathbf{b}_{i'}^{t_m+K}, \dots, \mathbf{b}_{i'}^{t_m+2K-2}),$$

we link them if the spatial overlap between  $\mathbf{b}_i^{t_m+K-1}$  and  $\mathbf{b}_{i'}^{t_m+K-1}$  from the temporally-overlapping frame (*i.e.* the same frame) is larger than a pre-defined threshold.

We perform a greedy short tubelet linking algorithm. Initially, we put the short tubelets from all short video segments into a pool and record the corresponding segment for each tubelet. Our algorithm pops out the short tubelet  $\mathcal{T}$  with the highest classification score from the pool. We check the IoU of the boxes over the temporally-overlapping frame between  $\mathcal{T}$  and its temporally-overlapping short tubelets. If the IoU is larger than a threshold, fixed as 0.4 in our implementation, we merge the two short tubelets into a single longer tubelet, remove the box with the lower score for the overlapping frame, update the classification score for the merged tubelet according to Eq. (2) for better classification, and record the corresponding segment (a combination of the corresponding two video segments). We then push the merged tubelet into the pool. This process is repeated until no more tubelets can be merged. Fig. 3 gives the examples of linking short tubelets to form long tubelets.

The tubelets remaining in the pool form the video object detection results: the score of the tubelet is assigned to each box in the tubelet, and the boxes from all the tubelets associated with a frame are regarded as the final detection boxes for the corresponding frame.

### 3.4. Implementation Details

**Cuboid Proposal.** The base network is ResNet-101 [11] pre-trained on the ImageNet classification dataset [26]: we remove all layers after the *Res5c* layer and replace the convolutional layers in the fifth block by dilated ones [1, 34] to reduce the stride from 32 to 16. On the basis of the base network, we add a convolutional layer with 512 filters of  $3 \times 3$ , and use two convolutional layers of  $1 \times 1$  to regress the offsets and predict the objectness scores for cuboid proposals. The network is split into two sub-networks: the first one has two residual blocks pass each frame separately to obtain frame-specific features which are concatenated as input of the second sub-network with three residual blocks.

We use four anchor scales  $64^2$ ,  $128^2$ ,  $256^2$ , and  $512^2$  with three aspect ratios 1:1, 1:2, and 2:1, resulting in 12 anchors at each location in total. The length  $K$  of each video segment will be studied in our experiments. The loss function is the same as that in the standard RPN [25]: the cross-entropy loss for classification and the smoothed L1 loss for regression. The training targets are the ground truth cuboids as defined in Eq. (1). The NMS threshold 0.7 is chosen and at most 300 proposals are kept for the detection network training/testing. In the testing stage, if the number of frames in the last segment is smaller than  $K$ , we pad the segment by some frames copied from the last frame.

**Short Tubelet Detection.** The base network is the same as it for cuboid proposal. We use ROI pooling to extract  $7 \times 7$  response maps from the layer *Res5c*, followed by two fully-connected + ReLU layers (1024 neurons). We use one fully-connected layer for classification and another fully-connected layer for bounding box regression. Following the Fast R-CNN [5], we train the network with online hard example mining [28]. The difference between our short tubelet detection training and the Fast R-CNN training is in the ground truth matching. In particular, we match a cuboid proposal to a ground truth box if the IoU between the cuboid proposal and a ground truth cuboid is larger than a threshold (typically 0.5). This is because the CPN is trained for cuboids, which makes cuboid proposals hard to match ground truth boxes directly. This matching strategy also ensures that a cuboid proposal corresponds to the same object in different frames. The training targets are still ground truth boxes (rather than ground truth cuboids) because we want to get accurate object locations in each frame. During testing, the T-NMS threshold is set to 0.4.

**Training.** We use SGD to train the cuboid proposal network and the short tubelet detection network. We initialize the

weights of the newly added layers by a zero-mean Gaussian distribution whose std is 0.01. Images are resized to shorter side 600 pixels for both training and testing. We set the mini-batch size to 8, the learning rate to  $1 \times 10^{-3}$  for the first 40K iterations and  $1 \times 10^{-4}$  for the next 20K iterations, and the momentum to 0.9. We do not find the gain from sharing the base networks for the cuboid proposal network and the short tubelet detection network, so we simply train them separately. Our implementation is based on the Caffe [13] deep learning framework on a TitanX (Pascal) GPU.

### 3.5. Discussions

**Action Detection.** The tasks of spatio-temporal action detection [7] and object detection in videos are similar to some extent. The purpose of spatio-temporal action detection is to localize and classify actions in each video frame. Some recent solutions [7, 12, 23, 27, 30, 14] to action becomes similar to video object detection and some of them can also be cast into the object/action linking framework. For instance, linking through neighboring frames, which is studied in video object detection [3, 16, 15, 17, 8], is also explored in [7, 12, 23, 27, 30]. We find that only the contemporary work [14] in action detection adopts the scheme of linking through temporally-overlapping frames, and its short tubelet detection scheme, similar to [15], is different from our cuboid proposal based method. It should be noted that although the solution frameworks of the two problems are similar in high level, the research focuses are different: action detection is more about capturing the motion from the temporal signals, whereas video object detection can be done in a single image with the temporal signal improving the classification quality. As validated in the later empirical results, the state-of-art action detection method [14], whose framework is similar to our method and [15, 3], performs poor in video object detection.

**Multi-object Issue.** It is possible that one cuboid contains multiple objects, because a cuboid tends to occupy a larger region than the object. However, as observed in our experiments, this problem has almost negligible influence on the detection performance. This is because our overlapping-based short tubelet linking can be accomplished when a video segment only has two frames. In this case, each cuboid, in most cases, contains only one object. It is worth noting that it is not necessary to use video segments longer than two frames, because short two-frame segments already support overlapping-based short tubelet linking.

**Boundary Issue.** It is possible that in a video segment, an object may not appear in all the frames. We investigate the VID dataset and find that this boundary issue only leads to small performance drop (up to 0.57%). As a future work, we will adopt the 1D belief propagation algorithm to optimally re-label the boxes for each frame in the linked tubelets to resolve the bounding issue.

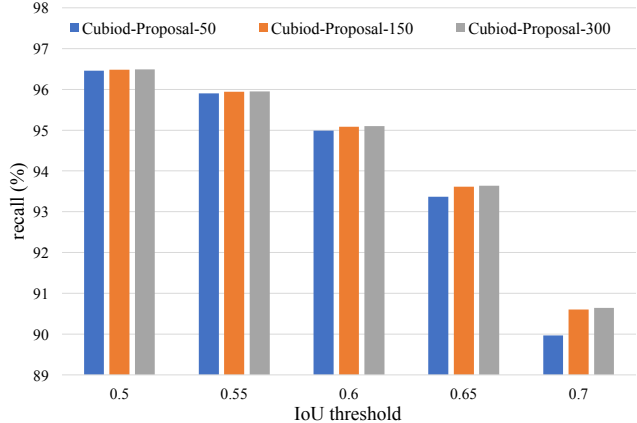


Figure 4. Recall vs. IoU threshold on the VID validation set. We show the results when keeping 50, 150, and 300 cuboid proposals for IoU threshold 0.5 to 0.7.

## 4. Experiments

### 4.1. Dataset and Evaluation Metric

We use the ImageNet VID dataset [26] which was introduced in the ILSVRC 2015 challenge. There are 30 object classes in the dataset which cover different movement types and different levels of clutteriness. The dataset has 5354 videos in total which are divided into training, validation, and testing subsets with 3862, 555, and 937 videos, respectively. Each video has about 300 frames on average. The dataset provides ground truth object locations, labels, and object identifications for each frame of the video. Since the annotations for the testing subset has been reserved for the challenge and the evaluation server has been closed, we test on the validation subset as most of the other works.

We use the classical detection evaluation metric for the VID dataset, *i.e.*, the Average Precision (AP) and mean of AP (mAP) over all classes, following the previous works tested on VID [3, 15, 16, 17, 36, 37].

### 4.2. Ablation Studies

We first conduct detailed ablation experiments to study the effectiveness of different settings in our method, including cuboid proposal recall, short tubelet detection, video segment length, NMS/T-NMS, and short tubelet linking. In particular, the static image detector baseline mentioned below is a Faster R-CNN network [25] that treats all frames as static images without considering temporal information.

**Cuboid Proposal Recall.** We first evaluate the recall of proposals by CPN. To do this, we generate a collection of cuboid proposals for each video segment and compute their recall at different IoU thresholds (0.5 to 0.7) with ground truth cuboids. Fig. 4 shows the quantitative results on the validation set. Firstly, we can see that keeping as few as 50 proposals already gives reasonably good performance:

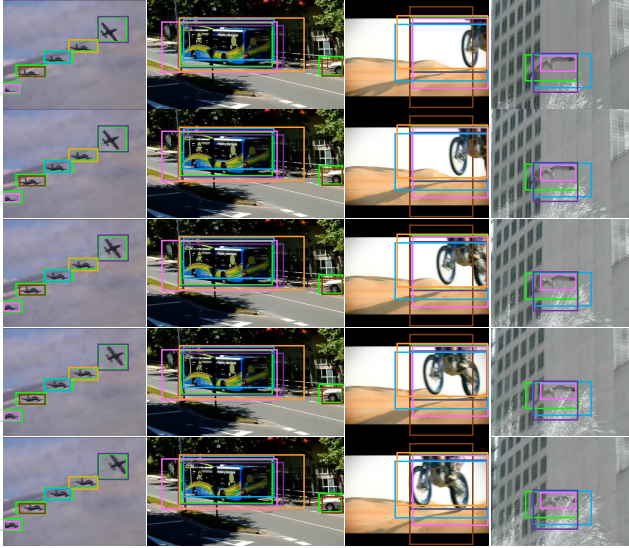


Figure 5. Visualization of some cuboid proposal results. Each column corresponds to a short video segment. The green boxes are the ground truths and the rest are the cuboid proposals. Boxes with the same color belong to the same cuboid proposals. For each video segment, we only show five proposals with the highest objectness scores for simplicity.

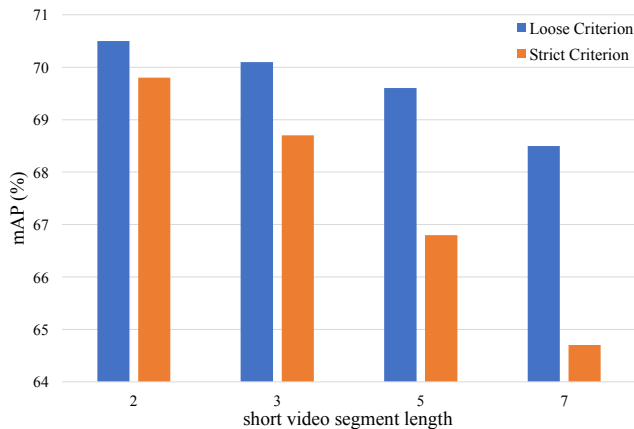


Figure 6. Short tubelet detection results. The “Loose Criterion” is the standard detection mAP and the “Strict Criterion” checks whether the instance IDs of the boxes in a tubelet are the same.

more than 96.46% of the ground truths are recalled for IoU 0.5. Secondly, increasing the number of proposals brings only marginal gains for lower IoU thresholds (*e.g.* 0.5) and gives larger gains for higher IoU thresholds (*e.g.* 0.7). The results show that choosing 300 proposals already achieves satisfactory recall. Thus we only use 300 proposals for following experiments. We also show several qualitative results in Fig. 5. The green boxes are the ground truths and the rest are the proposals generated by CPN. In most cases, there is at least one proposal that has sufficient overlap with the ground truths, which shows that the CPN can accurately learn the boundaries of the object movement. Take the aeroplane as an example, the boxes in the top figure touch the aeroplane tails while those in the bottom touch the aero-

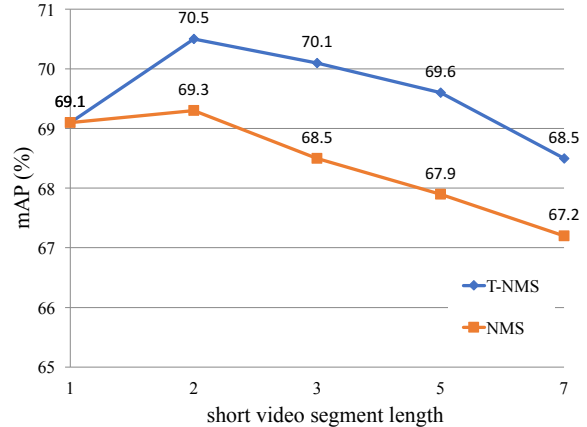


Figure 7. Detection results for NMS/T-NMS and different short video segment lengths. Video segment length 1 means the static image detector.

plane heads. Besides, it deals well with the videos having single/multiple, small/large, fast/slow moving objects.

**Short Tubelet Detection.** We then investigate whether the boxes in the short tubelets for short video segments correspond to the same objects. For a testing video, our method first generates a set of short tubelets. Then if all boxes in the short tubelet localize object accurately and correspond to the same object, the tubelet is classified as true positive, and otherwise it is a false positive. After that we compute the mAP. It is obvious that this is a more strict evaluation criterion than the one used for video object detection. Fig. 6 shows the results. We can see that using the strict evaluation protocol only slightly decreases the performance (*e.g.*, from 70.5% to 69.8% or from 70.1% to 68.7%), which justifies that the linking results of short tubelets are reasonably accurate.

**The Influence of Short Video Segment Length.** We discuss the influence of short video segment length. From Fig. 7, we can see that using video segment lengths of 2, 3, and 5 (with T-NMS) all improves over the static baseline. The largest improvement (1.4% mAP) is obtained when the video segment length is 2. When the video segment length increases, the performance decreases. In addition, as shown in Fig. 6, we can see that the short tubelet detection performance for long video segments is worse than short ones. There are several reasons explaining this phenomenon. First, longer segments are more probable to generate oversized proposals which have smaller overlap with the ground truth boxes in each frame. Second, the oversized proposals are probable to overlap with the image regions of other objects, causing more ambiguities for accurate localization and classification. Due to the better object/tubelet detection results, we set the video segment length to 2 in the following if not specified. In addition, the video segment length larger than 1 ensures that we can link objects in the same frame.

Table 1. Detection results (mAP in %) of different methods on the VID validation set which is divided into three subsets according to the object moving speed. The relative gains over the static image detector baseline (a) are listed in the subscript. The video segment length is set to 2 for (c-e).

Methods	(a)	(b)	(c)	(d)	(e)
Seq-NMS		✓			
CPN			✓	✓	✓
T-NMS				✓	✓
Short Tubelet Linking					✓
mAP (%)	69.1	70.9 <sub>↑1.8</sub>	69.3 <sub>↑0.2</sub>	70.5 <sub>↑1.4</sub>	<b>74.5<sub>↑5.4</sub></b>
mAP (%) (slow)	76.8	78.5 <sub>↑1.7</sub>	76.7 <sub>↓0.1</sub>	77.7 <sub>↑0.9</sub>	<b>80.4<sub>↑3.6</sub></b>
mAP (%) (medium)	68.5	70.4 <sub>↑1.9</sub>	68.9 <sub>↑0.4</sub>	70.2 <sub>↑1.7</sub>	<b>74.7<sub>↑6.2</sub></b>
mAP (%) (fast)	47.2	49.4 <sub>↑2.2</sub>	47.7 <sub>↑0.5</sub>	49.4 <sub>↑2.2</sub>	<b>56.0<sub>↑8.8</sub></b>

**NMS vs. T-NMS.** We study the influence of NMS/T-NMS for object detection. The NMS is implemented by removing boxes for each frame independently instead of removing short tubelets for video segments in the T-NMS. Fig. 7 and Table 1 show that T-NMS gives better performance than NMS, which confirms that compared with NMS handling each frame independently, simply considering short range temporal contexts contributes to better detection results.

**Short Tubelet Linking.** Here, we show the improvement by linking short tubelets. We evaluate the performance on slow, medium, and fast ones which are formed according to their speed as done in [36]. As we can see in Table 1, compared with the static baseline, considering both short and long range temporal information boosts the performance. When linking objects over the whole video to consider long range temporal context, there is significant improvements (5.4% to static and 4.0% to without short tubelet linking). Importantly, the performance gains are mainly from the faster objects (6.2% for medium and 8.8% for fast). It is natural that faster objects may have more variations, thus detecting them depends more on temporal context. As short tubelet linking performs much better than others, in the following we only report results by short tubelet linking.

**Ours vs. Seq-NMS [8].** We also compare our results with results by the linking in neighboring frames method Seq-NMS [8]. As shown in Table 1, the Seq-NMS obtains better performance than the static baseline, which also confirms the usefulness of temporal contexts. However, the Seq-NMS performs much worse than our method. In particular, the performance improvement for fast moving objects by Seq-NMS is only 2.2%, whereas our method obtains 8.8% improvement. This is because the same object in neighboring frames has different locations and appearances, which influences the quality of object linking, especially for fast moving objects. These results demonstrate the effectiveness of our linking in the same frame strategy.

**Comparison with the State-of-the-Art Action Detection Method [14].** Finally, we compare our result with the result from [14] which is the state-of-the-art solution in video action detection and adopts the object/action linking framework similar to our method and [15, 3, 16], by deploying the

method on VID. The result by [14] is 60.2% mAP which is much weaker than our 74.5%. The better performance of our method comes from that (1) the two problems, video object detection and action detection, are different, see Section 3.5, (2) the short range linking schemes are different: ours uses cuboid proposal whereas [14] uses cuboid anchor, and (3) the localization schemes are different: ours localizes objects for different frames separately, whereas [14] localizes actions for different frames jointly, which will result in poor localization performance.

### 4.3. Results

We compare our object detection results with the current state of the arts in Table 2. First, when only training on the VID dataset, our method obtains the superior result 74.5% mAP. To pursue the state-of-the-art detection performance, we follow the previous methods [3, 16, 36] to use the mixture of ImageNet VID and DET datasets for training the detection network, and utilize the standard multi-scale training and testing [10]. As we can see, comparing our 80.6% with other methods using the same ResNet-101 network [3, 36], our method also obtains better performance, which confirms the effectiveness of our linking strategy. Importantly, compared with [3, 36, 16, 15] that link objects in neighboring frames, our linking objects in the same frame strategy obtains better performance, which demonstrates that our method can obtain higher quality object linking results. In particular, Zhu *et al.* [36] combine feature propagation and the score propagation [8] to obtain 78.4% performance. Feichtenhofer *et al.* [3] add a tracking loss to learn better features for performance improvement. There are potential benefits from learning better features in the proposal and detection stages by incorporating other methods such as feature propagation and extra losses into our method.

Fig. 8 visualizes several detection result comparisons between the static image detector and our method. From the first two rows, we can see that the static method fails to detect the red-panda when there are severe motion blurs and occlusions. This is reasonable because the appearance features have been severely degraded in this situation. After applying the object linking and rescoring, our method successfully classifies the target in the challenging frames. In addition, it is common that the static detectors may confuse with similar classes (*e.g.*, bikes *vs.* motor-bikes, cats *vs.* dogs) especially when a frame has low image quality. This problem can also be alleviated by rescoring the detections in the whole video because some frames have correct classifications and can propagate these scores to the challenging frames by object linking.

### 4.4. Runtime

For the case of two frame segments, our method takes 0.35s per-frame for testing which is comparable to 0.30s

Table 2. Average precision (in %) for different methods on the VID dataset. \* indicates models trained on the mixture of VID and DET datasets.

Method	aero	antelope	bear	bike	bird	bus	car	cattle	dog	cat	elephant	fox	g_panda	hamster	horse	
Kang <i>et al.</i> [15]	84.6	78.1	72.0	67.2	68.0	80.1	54.7	61.2	61.6	78.9	71.6	83.2	78.1	91.5	66.8	
Kang <i>et al.</i> [16]*	83.7	<b>85.7</b>	84.4	74.5	73.8	75.7	57.1	58.7	72.3	69.2	80.2	83.4	80.5	93.1	<b>84.2</b>	
Lee <i>et al.</i> [20]*	86.3	83.4	88.2	<b>78.9</b>	65.9	<b>90.6</b>	<b>66.3</b>	<b>81.5</b>	72.1	76.8	82.4	88.9	<b>91.3</b>	89.3	66.5	
Zhu <i>et al.</i> [36]*	-	-	-	-	-	-	-	-	-	-	-	-	-	-	-	
Feichtenhofer <i>et al.</i> [3]*	90.2	82.3	87.9	70.1	73.2	87.7	57.0	80.6	77.3	82.6	<b>83.0</b>	<b>97.8</b>	85.8	96.6	82.1	
Ours	89.9	77.8	81.7	71.6	71.9	85.3	60.0	69.9	69.4	85.7	79.9	90.2	83.4	93.5	67.3	
Ours*	<b>90.5</b>	80.1	<b>89.0</b>	75.7	<b>75.5</b>	83.5	64.0	71.4	<b>81.3</b>	<b>92.3</b>	80.0	96.1	87.6	<b>97.8</b>	77.5	
Method	lion	lizard	monkey	mbike	rabbit	r_panda	sheep	snake	squirrel	tiger	train	turtle	boat	whale	zebra	mAP
Kang <i>et al.</i> [15]	21.6	74.4	36.6	76.3	51.4	70.6	64.2	61.2	42.3	84.8	78.1	77.2	61.5	66.9	88.5	68.4
Kang <i>et al.</i> [16]*	67.8	80.3	54.8	80.6	63.7	85.7	60.5	72.9	52.7	89.7	81.3	73.7	69.5	33.5	90.2	73.8
Lee <i>et al.</i> [20]*	38.0	77.1	57.3	<b>88.8</b>	78.2	77.7	40.6	50.3	44.3	91.8	78.2	75.1	<b>81.7</b>	63.1	85.2	74.5
Zhu <i>et al.</i> [36]*	-	-	-	-	-	-	-	-	-	-	-	-	-	-	-	78.4
Feichtenhofer <i>et al.</i> [3]*	66.7	<b>83.4</b>	<b>57.6</b>	86.7	74.2	<b>91.6</b>	59.7	76.4	<b>68.4</b>	<b>92.6</b>	<b>86.1</b>	<b>84.3</b>	69.7	66.3	<b>95.2</b>	79.8
Ours	46.9	74.7	49.2	81.4	57.0	74.9	65.2	60.0	48.6	91.0	85.1	82.7	74.0	74.9	91.7	74.5
Ours*	<b>73.1</b>	81.5	56.0	85.7	<b>79.9</b>	87.0	<b>68.8</b>	<b>80.7</b>	61.6	91.6	85.5	81.3	73.6	<b>77.4</b>	91.9	<b>80.6</b>



Figure 8. Example detection results of the static detector and our method (only the top-scoring boxes around objects are shown). Each row shows the results of sampled successive frames. For the linking results, boxes with the same color belong to the same tubelet in the video. Our method outperforms the static image detector when there are motion blurs, video defocus, and occlusions in the video.

by the static baseline. The small extra cost comes from the cuboid proposal generation procedure: a small sub-network processing the two frames separately. The extra time cost is small for the detection stage due to the shared convolutional feature map, the computation time of T-NMS is almost the same as the NMS, and the short tubelet linking is very efficient (about 10ms per-frame). The speed becomes even faster than the baseline when the short video segment length is larger than 2 (e.g., 0.27s and 0.23s for video segment length 3 and 5 respectively), because the CPN generates cuboid proposals for all the frames in the segment by

computing the features once.

## 5. Conclusion

In this paper, we explore to link objects in the same frame for high quality object linking to improve the classification quality. Our method has three main components to achieve our goal: (1) cuboid proposal network, (2) short tubelet detection, and (3) short tubelet linking. Our method obtains the state-of-the-art video detection performance on the VID dataset.



## References

- [1] L.-C. Chen, G. Papandreou, I. Kokkinos, K. Murphy, and A. L. Yuille. Deeplab: Semantic image segmentation with deep convolutional nets, atrous convolution, and fully connected crfs. *TPAMI*, 2017. 4
- [2] A. Dosovitskiy, P. Fischer, E. Ilg, P. Hausser, C. Hazirbas, V. Golkov, P. van der Smagt, D. Cremers, and T. Brox. FlowNet: Learning optical flow with convolutional networks. In *ICCV*, pages 2758–2766, 2015. 2
- [3] C. Feichtenhofer, A. Pinz, and A. Zisserman. Detect to track and track to detect. In *ICCV*, pages 3038–3046, 2017. 1, 2, 5, 7, 8
- [4] P. F. Felzenszwalb, R. B. Girshick, D. McAllester, and D. Ramanan. Object detection with discriminatively trained part-based models. *TPAMI*, 32(9):1627–1645, 2010. 2
- [5] R. Girshick. Fast r-cnn. In *ICCV*, pages 1440–1448, 2015. 1, 2, 3, 4
- [6] R. Girshick, J. Donahue, T. Darrell, and J. Malik. Rich feature hierarchies for accurate object detection and semantic segmentation. In *CVPR*, pages 580–587, 2014. 1, 2
- [7] G. Gkioxari and J. Malik. Finding action tubes. In *CVPR*, pages 759–768, 2015. 5
- [8] W. Han, P. Khorrami, T. L. Paine, P. Ramachandran, M. Babaeizadeh, H. Shi, J. Li, S. Yan, and T. S. Huang. Seq-nms for video object detection. *arXiv preprint arXiv:1602.08465*, 2016. 1, 2, 5, 7
- [9] K. He, G. Gkioxari, P. Dollar, and R. Girshick. Mask r-cnn. In *ICCV*, pages 2961–2969, 2017. 2
- [10] K. He, X. Zhang, S. Ren, and J. Sun. Spatial pyramid pooling in deep convolutional networks for visual recognition. *TPAMI*, 37(9):1904–1916, 2015. 7
- [11] K. He, X. Zhang, S. Ren, and J. Sun. Deep residual learning for image recognition. In *CVPR*, pages 770–778, 2016. 1, 4
- [12] R. Hou, C. Chen, and M. Shah. Tube convolutional neural network (t-cnn) for action detection in videos. In *ICCV*, pages 5822–5831, 2017. 5
- [13] Y. Jia, E. Shelhamer, J. Donahue, S. Karayev, J. Long, R. Girshick, S. Guadarrama, and T. Darrell. Caffe: Convolutional architecture for fast feature embedding. In *ACM MM*, pages 675–678, 2014. 5
- [14] V. Kalogeiton, P. Weinzaepfel, V. Ferrari, and C. Schmid. Action tubelet detector for spatio-temporal action localization. In *ICCV*, pages 4405–4413, 2017. 5, 7
- [15] K. Kang, H. Li, T. Xiao, W. Ouyang, J. Yan, X. Liu, and X. Wang. Object detection in videos with tubelet proposal networks. In *CVPR*, pages 727–735, 2017. 1, 2, 5, 7, 8
- [16] K. Kang, H. Li, J. Yan, X. Zeng, B. Yang, T. Xiao, C. Zhang, Z. Wang, R. Wang, X. Wang, et al. T-cnn: Tubelets with convolutional neural networks for object detection from videos. *arXiv preprint arXiv:1604.02532*, 2016. 1, 2, 5, 7, 8
- [17] K. Kang, W. Ouyang, H. Li, and X. Wang. Object detection from video tubelets with convolutional neural networks. In *CVPR*, pages 817–825, 2016. 1, 2, 5
- [18] A. Krizhevsky, I. Sutskever, and G. E. Hinton. Imagenet classification with deep convolutional neural networks. In *NIPS*, pages 1097–1105, 2012. 1
- [19] Y. LeCun, L. Bottou, Y. Bengio, and P. Haffner. Gradient-based learning applied to document recognition. *Proceedings of the IEEE*, 86(11):2278–2324, 1998. 1
- [20] B. Lee, E. Erdenee, S. Jin, M. Y. Nam, Y. G. Jung, and P. K. Rhee. Multi-class multi-object tracking using changing point detection. In *ECCV*, pages 68–83, 2016. 8
- [21] T.-Y. Lin, P. Goyal, R. Girshick, K. He, and P. Dollar. Focal loss for dense object detection. In *ICCV*, pages 2980–2988, 2017. 2
- [22] W. Liu, D. Anguelov, D. Erhan, C. Szegedy, S. Reed, C.-Y. Fu, and A. C. Berg. Ssd: Single shot multibox detector. In *ECCV*, pages 21–37, 2016. 1, 2
- [23] X. Peng and C. Schmid. Multi-region two-stream r-cnn for action detection. In *ECCV*, pages 744–759, 2016. 5
- [24] J. Redmon, S. Divvala, R. Girshick, and A. Farhadi. You only look once: Unified, real-time object detection. In *CVPR*, pages 779–788, 2016. 1, 2
- [25] S. Ren, K. He, R. Girshick, and J. Sun. Faster r-cnn: Towards real-time object detection with region proposal networks. In *NIPS*, pages 91–99, 2015. 1, 3, 4, 5
- [26] O. Russakovsky, J. Deng, H. Su, J. Krause, S. Satheesh, S. Ma, Z. Huang, A. Karpathy, A. Khosla, M. Bernstein, et al. Imagenet large scale visual recognition challenge. *IJCV*, 115(3):211–252, 2015. 2, 4, 5
- [27] S. Saha, G. Singh, and F. Cuzzolin. Amtnet: Action-microtube regression by end-to-end trainable deep architecture. In *ICCV*, pages 4414–4423, 2017. 5
- [28] A. Shrivastava, A. Gupta, and R. Girshick. Training region-based object detectors with online hard example mining. In *CVPR*, pages 761–769, 2016. 4
- [29] K. Simonyan and A. Zisserman. Very deep convolutional networks for large-scale image recognition. In *ICLR*, 2015. 1
- [30] G. Singh, S. Saha, M. Sapienza, P. Torr, and F. Cuzzolin. Online real-time multiple spatiotemporal action localisation and prediction. In *ICCV*, pages 3637–3646, 2017. 5
- [31] P. Tang, X. Wang, X. Bai, and W. Liu. Multiple instance detection network with online instance classifier refinement. In *CVPR*, pages 2843–2851, 2017. 1
- [32] P. Viola and M. Jones. Rapid object detection using a boosted cascade of simple features. In *CVPR*, 2001. 2
- [33] L. Wang, W. Ouyang, X. Wang, and H. Lu. Visual tracking with fully convolutional networks. In *ICCV*, pages 3119–3127, 2015. 2
- [34] F. Yu and V. Koltun. Multi-scale context aggregation by dilated convolutions. In *ICLR*, 2016. 4
- [35] Z. Zhang, S. Qiao, C. Xie, W. Shen, B. Wang, and A. L. Yuille. Single-shot object detection with enriched semantics. In *CVPR*, 2018. 1
- [36] X. Zhu, Y. Wang, J. Dai, L. Yuan, and Y. Wei. Flow-guided feature aggregation for video object detection. In *ICCV*, pages 408–417, 2017. 1, 2, 5, 7, 8
- [37] X. Zhu, Y. Xiong, J. Dai, L. Yuan, and Y. Wei. Deep feature flow for video recognition. In *CVPR*, pages 2349–2358, 2017. 1, 2, 5